

**A NUMERICAL STUDY OF FLOW DYNAMICS  
IN THE STARTING PHASES OF LAMINAR  
SUBSONIC AND SUPERSONIC ROUND JETS**

**HAROON AHMAD**



**DEPARTMENT OF APPLIED MECHANICS  
INDIAN INSTITUTE OF TECHNOLOGY DELHI**

**February 2022**

©Indian Institute of Technology Delhi (IITD), New Delhi, 2022

# A NUMERICAL STUDY OF FLOW DYNAMICS IN THE STARTING PHASES OF LAMINAR SUBSONIC AND SUPERSONIC ROUND JETS

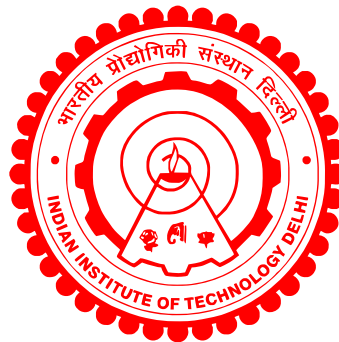
by

**HAROON AHMAD**

Department of Applied Mechanics

Submitted

in fulfillment of the requirements of the degree of Doctor of Philosophy  
to the



**INDIAN INSTITUTE OF TECHNOLOGY DELHI**

**February 2022**

---

## CERTIFICATE

This is to certify that the thesis entitled “**A Numerical Study of Flow Dynamics in the Starting Phases of Laminar Subsonic and Supersonic Round Jets**” is being submitted by **Haroon Ahmad** to the *Indian Institute of Technology Delhi* for the award of the degree of **Doctor of Philosophy**, is a record of the bonafide research work carried out by him and has been prepared under our guidance and supervision in conformity with the rules and regulations of the Indian Institute of Technology Delhi. The research reports and results contained in this thesis have not been submitted, in part or in full, to any other university or institute for the award of any degree or diploma.

**Prof. SANJEEV SANGHI**

Applied Mechanics Department  
Indian Institute of Technology Delhi  
Hauz Khaz, New Delhi-110016  
New Delhi, India

**Prof. NADEEM HASAN**

Department of Mechanical Engineering  
Zakir Hussain College of Engineering and Technology  
Aligarh Muslim University  
Aligarh-202002  
U.P., India

*dedicated to my mother Mrs. Shagufta Jabeen and to all those who taught me.*

## ACKNOWLEDGEMENT

Praise and Thanks to the Almighty God who guided me in every stage of life and in this research work. This research work has been possible due to my supervisor Prof. Sanjeev Sanghi to whom I am very grateful. He selected me under his able supervision, gave me this problem and guided me in the course of this research work. Prof. Nadeem Hasan resolved various issues related with the development of the code which were the real road-blocks in our work and through his God-gifted brilliance developed the idea of PVU-M+J scheme which, according to me, is the most significant contribution of this research work. He not only taught me the debugging of CFD solvers but also the basic research methodology to investigate the fluid mechanics problems. Without him this work would have never been completed and certainly would have been an oblivion. I would also like to thank members of my research committee *i.e.* Prof. Anupam Dewan, Dr. Sawan Suman and Dr. Supreet Singh Bahga for their comments, suggestions and encouragement in this work. I also thank my friends Dr. Anubhav Rawat, Dr. Pritanshu Ranjan, Dr. Sagar Saroha, Dr. Lokesh Ragata, Dr. Hamid Hassan Khan, Dr. Anuj Kumar Shukla, Dr. Bishweshwar Babu, Dr. Sartaj Tanweer, Dr. Reyaz Arif, Dr. Mohammed Khalid, Dr. Mohammed Furqan, Mr. Mohammed Suhail Naim and Mr. Obaidullah Khawar who helped me and supported me in every aspect during the course of this work, without them completion of this work would have been very difficult. I am very much thankful to Mr. Parvaez Ahmad for teaching me the MPI parallel programming which enabled me to develop the solver. I am thankful to my friends, Dr. Wasiuddin and Dr. P.M.G. Bashir Asdaque, who helped and supported me in every possible manner during my stay in New Delhi. I am thankful to my teacher Dr. Mohammed Shoeb who guided me in every stage of life. I am also very thankful to my mother Shagufta Jabeen and to my uncles Dr. Ejaz-un-Nabi, Mr. Jawed Nizami and Mr. Junaid Nizami, without them I would have never reached here.

## ABSTRACT

Numerical investigation of the flow dynamics in the starting phases of laminar, axisymmetric, continuously blowing compressible jets is performed. The effect of jet Reynolds number ( $Re_j$ ), jet Mach number ( $M_j$ ), pressure-ratio ( $\frac{p_j}{p_a}$ ) and velocity ratio ( $\frac{U_a}{U_j}$ ) on the different starting flow structures and their flow dynamics is explored. The Navier Stokes solver employs the novel *PVU-M+J* scheme developed in this study for the simulations of the compressible jets. The *PVU-M+J* scheme is a variant of the existing *PVU-M+* scheme[1]. The simulations show the starting flow structures obtained for the limiting case of a top-hat profile at the orifice/short nozzle exit. Core bow shock is formed in the inviscid core of the transonic/supersonic jets for sustaining the supersonic flow-field in the primary vortex ring (*PVR*). The embedded shock (*ES*) and vortex induced shock (*VIS*) are also found to sustain the evolving *PVR* in the supersonic jets and at high magnitudes of  $\frac{U_a}{U_j}$  these shocks may even cease to form inside the *PVR* which has shrunked to a circular shape. The formation of Kelvin-Helmholtz vortices (*KHV*) leads to the pinch-off of the *PVR* from the trailing shear layer which is also responsible for the quasi-constancy of the *PVR* circulation. For supersonic jets with  $\frac{p_j}{p_a} \leq 1$ , *KHV* entrained into *PVR* interact with the *ES* to cause a shock-vortex interaction which results in the appearance of multiple *VIS*. It is established that the different events of interaction of *KHV* with the *ES* inside the *PVR* after the pinch-off are a manifestation of two factors; (i) the constraint imposed on the *PVR* by quasi time-invariance of circulation around a material curve enclosing the *PVR* and, (ii) the requirement of spatially-cyclic property distribution inside the *PVR*. In the under-expanded jets ( $\frac{p_j}{p_a} > 1$ ), the investigation of the shock-shear layer-vortex interaction (*SSVI*) shows that the refracted oblique shock portion, across the shear layer, inside the *PVR* evolves in response to the vorticity dynamics prevailing in the evolving *PVR*. This is found to be the main reason for the observed oblique shock refraction in *SSVI*. For under-expanded jets, apart from Mach-reflection time-scale of the *CRVR* pattern formation is also governed by the initial strength of the slip-stream which in turn is regulated by all the four parameters *i.e.*  $Re_j$ ,  $M_j$ ,  $\frac{p_j}{p_a}$  and  $\frac{U_a}{U_j}$ . If the slip-stream strength is very low, the *CRVR* formation is completely suppressed. While for high magnitudes of slip-stream strength there is formation of multiple *CRVRs*. The *CRVR* evolution involves the rolling of *CRVR* over the *PVR* periphery followed by the shock-vortex interaction between *CRVR* and vortex induced shock (*VIS*) of the *PVR*. In the under-expanded jets, *PVR* and *CRVR* circulations attain quasi-constancy as the *CRVR* starts to roll over the *PVR* periphery. The *PVR* circulation is shown to attain quasi-constancy even in the absence of its pinch-off (detachment) from the

shear layer. The slip-stream strength is found to govern the magnitude of *CRVR* circulation. New type of discontinuities (induced shocks and vortex sheet) are observed inside the *CRVRs* generated from medium/high strength slip-streams. The self roll-up of *CRVR* causes the formation of the transient spiral stagnation point and the vortex sheet which leads to the formation of the transient saddle stagnation point. The formation of induced shocks inside these *CRVRs* is due to the combination of two different constraints *i.e.* (a) cyclic distribution of fluid properties inside the *CRVR* and (b) quasi-constancy of the *CRVR* circulation. The shock-vortex interaction between *CRVR* and *VIS* is shown to be a weak shock-strong vortex interaction which occurs under the constraint of quasi-constancy of net-circulation enclosing both vortex rings (*i.e.* *PVR* & *CRVR*) and causes the weakening of *VIS*. The vorticity analysis of under-expanded jets with co-flow shows that with increase in co-flow ( $\frac{U_a}{U_j} > 0.15$ ), the *PVR* circulation attains quasi-constancy owing to the *PVR* pinch-off and shock-vortex interaction between KHV and ES. While, at low velocity ratio ( $0 \leq \frac{U_a}{U_j} \leq 0.15$ ), the quasi-constancy of *PVR* is attained due to the occurrence of shock-shear layer-vortex interaction (SSVI).

## सार

लैमिनार, एक्सिसिमेट्रिक, निरंतर धाराप्रवाह कंप्रेसिबल जेट्स के प्रारंभिक चरणों में प्रवाह गतिकी की संख्यात्मक जांच की गई है। विभिन्न प्रारंभिक प्रवाह संरचनाओं और उनके प्रवाह गतिकी पर जेट-रेनॉल्ड्स संख्या, जेट मच संख्या, दबाव अनुपात और वेग अनुपात के प्रभाव का पता लगाया जाता है। नेवियर स्टोक्स सॉल्वर ने इस अध्ययन में नवविकसित पीवीयू-एम+ जे संख्यात्मक स्कीम का उपयोग कंप्रेसिबल जेट्स के अनुकरण के लिए किया है। पीवीयू-एम+ जे संख्यात्मक स्कीम एक नवविकसित प्रकार है वर्तमान पीवीयू-एम+ संख्यात्मक स्कीम कि। वर्तमान अनुकरणों में प्रारंभिक प्रवाह संरचनाओं को छिद्र/शॉर्ट नोजल निकास पर एक टॉप-हैट प्रोफाइल के लिए प्राप्त किया गया। ट्रांसोनिक/सुपरसोनिक जेट के इनविसिड कोर में कोर बो शॉक बनता है जिसका कार्य प्राथमिक भंवर वलय में सुपरसोनिक प्रवाह-क्षेत्र को बनाए रखना है। एम्बेडेड शॉक और चक्रवात प्रेरित शॉक का निर्माण भी सुपरसोनिक जेट में विकसित प्राथमिक चक्रवात वलय को बनाए रखने के लिए होता है और वेग अनुपात की उच्च संख्या पर ये शॉक, प्राथमिक चक्रवात वलय के अंदर बनना बंद भी कर सकते हैं जो स्वयं एक गोलाकार आकार में सिकुड़ गया है। केल्विन-हेल्महोल्ट्ज़ चक्रवात के गठन से अनुगामी अपरूपण परत से प्राथमिक चक्रवात वलय का पिंच-ऑफ (विच्छिन्न) होता है जो प्राथमिक चक्रवात वलय के परिसंचरण की अर्ध-स्थिरता के लिए भी उत्तरदायी होता है। दबाव अनुपात  $\leq 1$  वाले सुपरसोनिक जेट के लिए, केल्विन-हेल्महोल्ट्ज़ चक्रवात प्राथमिक चक्रवात वलय में प्रविष्ट होते हैं और एम्बेडेड शॉक से परस्पर क्रियावृत होते हैं जिसके कारण एक शॉक-चक्रवात अंतःक्रिया होती है जिसके परिणामस्वरूप विभिन्न चक्रवात प्रेरित शॉक का निर्माण होता है। यह स्थापित किया गया है कि प्राथमिक चक्रवात वलय के अंदर एम्बेडेड शॉक के साथ केल्विन-हेल्महोल्ट्ज़ चक्रवात की परस्पर क्रियावृत्ति की विभिन्न घटनाएं पिंच-ऑफ के बाद दो कारकों की अभिव्यक्ति होती है; (i) प्राथमिक चक्रवात वलय को घेरने वाले सामग्री वक्र के चारों ओर परिसंचरण के अर्ध-समय-परिवर्तन द्वारा प्राथमिक चक्रवात वलय पर लगाया गया अवरोध और, (ii) प्राथमिक चक्रवात वलय के अंदर स्थानिक-चक्रीय संपत्ति वितरण की आवश्यकता। कम-विस्तारित जेट में, शॉक-अपरूपण परत-चक्रवात अंतःक्रिया की जांच से पता चलता है कि अपवर्तित परोक्ष शॉक भाग, अपरूपण परत के आर-पार, विकसित हो रहे प्राथमिक चक्रवात वलय में व्याप्त चक्रवात गतिकी की प्रतिक्रिया में विकसित होता है। यह शॉक-अपरूपण परत-चक्रवात अंतःक्रिया में परोक्ष शॉक के अपवर्तन का मुख्य कारण पाया गया है। कम-विस्तारित जेट के लिए, माक-प्रतिबिंब की समय-अवधि के अलावा विपरीत घूर्णन चक्रवात वलय प्रतिरूप का गठन स्लिप-स्ट्रीम की प्रारंभिक शक्ति द्वारा भी नियंत्रित होता है जो बदले में सभी चार मापदंडों द्वारा नियंत्रित होता है अर्थात् जेट-रेनॉल्ड्स संख्या, जेट मच संख्या, दबाव अनुपात एवम् वेग अनुपात। यदि स्लिप-स्ट्रीम की शक्ति बहुत कम है, तो विपरीत घूर्णन चक्रवात वलय का गठन पूरी तरह से समाप्त हो जाता है। जबकि उच्च स्लिप-स्ट्रीम शक्ति के लिए अनेक विपरीत घूर्णन चक्रवात वलय का गठन होता है। विपरीत घूर्णन चक्रवात वलय

क्रमागत उन्नति में प्राथमिक चक्रवात वलय परिधि पर विपरीत घूर्णन चक्रवात वलय का लुढ़कना शामिल है जिसके बाद विपरीत घूर्णन चक्रवात वलय और प्राथमिक चक्रवात वलय के चक्रवात प्रेरित शॉक के बीच शॉक-चक्रवात अंतःक्रिया शामिल है। कम-विस्तारित जेट में, विपरीत घूर्णन चक्रवात वलय और प्राथमिक चक्रवात वलय परिसंचरण अर्ध-स्थिरता प्राप्त करते हैं जैसे ही विपरीत घूर्णन चक्रवात वलय प्राथमिक चक्रवात वलय की परिधि पर लुढ़कना शुरू करता है। प्राथमिक चक्रवात वलय परिसंचरण को अपरूपण परत से पिंच-ऑफ के अभाव में भी अर्ध-स्थिरता प्राप्त करते दिखाया गया है। स्लिप-स्ट्रीम की शक्ति विपरीत घूर्णन चक्रवात वलय परिसंचरण को नियंत्रित करते पाई गई है। मध्यम/उच्च शक्ति वाली स्लिप-स्ट्रीम से उत्पन्न विपरीत घूर्णन चक्रवात वलय के अंदर नए प्रकार के अनिरंतरताए (प्रेरित शॉक और चक्रवात पत्र) देखे गए हैं। विपरीत घूर्णन चक्रवात वलय के स्वतः रोल-अप से क्षणिक सर्पिल ठहराव बिंदु और चक्रवात पत्र का निर्माण होता है जो क्षणिक सैडल ठहराव बिंदु के गठन की ओर जाता है। इन विपरीत घूर्णन चक्रवात वलय के अंदर प्रेरित झटकों का निर्माण दो अलग-अलग प्रतिबंधों के संयोजन के कारण होता है अर्थात् (1) विपरीत घूर्णन चक्रवात वलय के अंदर द्रव गुणों का चक्रीय वितरण और (2) विपरीत घूर्णन चक्रवात वलय परिसंचरण की अर्ध-स्थिरता। विपरीत घूर्णन चक्रवात वलय और चक्रवात प्रेरित शॉक के बीच शॉक-चक्रवात अंतःक्रिया को दुर्बल शॉक-दृढ़ चक्रवात अंतःक्रिया के रूप में दिखाया गया है जो दोनों चक्रवातों के चक्रों को घेरने वाले मूल-परिसंचरण की अर्ध-स्थिरता की प्रतिबंध के तहत होता है और चक्रवात प्रेरित शॉक के दुर्बल होने का कारण बनता है। सह-प्रवाह के साथ कम-विस्तारित जेट के चक्रवातिय विश्लेषण से पता चलता है कि सह-प्रवाह में वृद्धि के साथ (वेग अनुपात  $>0.15$ ), प्राथमिक चक्रवात वलय पिंच-ऑफ और केल्विन-हेल्महोल्ट्ज़ चक्रवात ऐवः एम्बेडेड शॉक के बीच शॉक-चक्रवात अंतःक्रिया के कारण प्राथमिक चक्रवात वलय परिसंचरण अर्ध-स्थिरता प्राप्त करता है। जबकि, कम वेग अनुपात पर ( $0 < \text{वेग अनुपात} < 0.15$ ), प्राथमिक चक्रवात वलय परिसंचरण की अर्ध-स्थिरता शॉक-अपरूपण परत-चक्रवात अंतःक्रिया के कारण प्राप्त होती है।

# Contents

<b>1</b>	<b>Introduction</b>	<b>1</b>
1.1	The compressible jet in starting phases . . . . .	1
1.2	Literature Review . . . . .	4
1.3	Conclusions from literature survey . . . . .	11
1.4	Open Questions and Problem Statement . . . . .	13
<b>2</b>	<b>Mathematical Formulation and Computational Methodology</b>	<b>15</b>
2.1	Governing Equations . . . . .	16
2.1.1	Basic form of the system of equations . . . . .	16
2.1.2	Thermodynamic model . . . . .	17
2.1.3	Scales for non-dimensionalization and the non-dimensional parameters . . . . .	19
2.1.4	Treatment of polar coordinate singularity . . . . .	21
2.1.5	Non-dimensional governing equations in the user defined polar-coordinate system . . . . .	22
2.2	Physical domain and Computational grid . . . . .	25
2.3	Initial conditions . . . . .	27
2.4	Artificial boundary conditions . . . . .	28
2.5	Numerical Scheme and Discretisation . . . . .	30
2.5.1	Basic approach of the PVU-M+J scheme . . . . .	32
2.5.2	Estimation of the convective fluxes in multi-dimensional flows . . . . .	33
2.5.3	Estimation of the non-convective viscous fluxes . . . . .	38
2.5.4	Estimation of the source term . . . . .	39
2.5.5	Numerical treatment of terms containing $\frac{1}{r}$ near $\tilde{r} = 0$ . . . . .	41
2.6	Filtering of the numerics to avoid grid-scale oscillations . . . . .	42
2.7	Performance of PVU-M+J scheme in the simulations of compressible jets	43
2.7.1	Simulations of the compressible jets from PVU-M+ scheme . . . . .	44
2.7.2	Improvements caused by the treatment of convective fluxes only . . . . .	47
2.7.3	Remedy in the estimation of viscous fluxes . . . . .	47

2.8	Validation . . . . .	50
<b>3</b>	<b>Primary Vortex Ring: Sustenance and Evolution</b>	<b>61</b>
3.1	Discontinuities that sustain the Primary Vortex Ring (PVR) . . . . .	62
3.1.1	Core bow shock (CBS), its formation and characteristics . . . . .	62
3.1.2	Embedded shock (ES) and vortex induced shock (VIS), their formation and characteristics . . . . .	69
3.2	Interaction of K-H vortices with the evolving PVR . . . . .	72
3.2.1	Circulation of the PVR . . . . .	72
3.2.2	Interaction of K-H vortices with ES and formation of multiple VIS . . . . .	76
3.2.3	Phenomenological model of the PVR evolution after pinch-off . . . . .	80
3.3	Shock-shear layer-vortex interaction . . . . .	85
3.3.1	Basic phenomenon . . . . .	85
3.3.2	Results from oblique shock theory . . . . .	89
3.3.3	Effect of $Re_j$ , $M_j$ and $\frac{p_j}{p_a}$ on the shock-shear layer-vortex interaction . . . . .	89
<b>4</b>	<b>Counter Rotating Vortex Rings: Formation and Evolution</b>	<b>92</b>
4.1	The formation of counter rotating vortex rings . . . . .	93
4.1.1	Effect of $Re_j$ , $M_j$ and $\frac{p_j}{p_a}$ on the slip-stream strength . . . . .	93
4.1.2	Effect of $\frac{p_j}{p_a}$ and $Re_j$ on CRVR formation . . . . .	95
4.1.3	Effect of $M_j$ on CRVR formation . . . . .	103
4.1.4	Phenomenological model governing the formation of single/multiple CRVRs and continuous emission of CRVRs . . . . .	104
4.2	The rolling of CRVR over the PVR periphery . . . . .	106
<b>5</b>	<b>Circulation and Vorticity Dynamics of PVR and CRVR during CRVR Evolution</b>	<b>112</b>
5.1	Circulation of the PVR and CRVR . . . . .	113
5.2	Quasi-constancy of the PVR circulation without vortex pinch-off . . . . .	118
5.2.1	Quasi-constancy of PVR circulation via formation and entrainment of secondary slip-stream in the PVR of moderately under-expanded jets . . . . .	118
5.2.2	Quasi-constancy of PVR circulation via shock-shear layer-vortex interaction in the PVR of highly under-expanded jets . . . . .	121
5.3	Formation of multiple discontinuities inside the CRVRs produced by high strength slip-streams . . . . .	123
5.3.1	Induced shock and vortex sheet . . . . .	123

5.3.2	Mechanism governing the formation of vortex sheet and induced shocks . . . . .	129
5.4	Interaction between CRVR and vortex induced shock (VIS) of the PVR	133
<b>6</b>	<b>Influence of Co-Flow on the Formation of Shocks and Vortex Rings in Under-Expanded Jets</b>	<b>141</b>
6.1	Effect of co-flow on embedded shock (ES) and vortex induced shock (VIS)	143
6.2	Effect of co-flow on Mach reflection and CRVR formation . . . . .	150
6.2.1	In moderately under-expanded jets . . . . .	150
6.2.2	In highly under-expanded jets . . . . .	155
6.2.3	Effect of co-flow on the physical mechanism governing CRVR formation . . . . .	159
6.3	Effect of co-flow on Primary Vortex Ring (PVR) . . . . .	160
6.3.1	Circulation and vorticity of the PVR . . . . .	160
6.3.2	Physics governing the quasi-constancy of PVR circulation . . . .	163
<b>7</b>	<b>Conclusions and Future Work</b>	<b>171</b>
<b>A</b>	<b>Grid independence study</b>	<b>177</b>
<b>B</b>	<b>Computation of average azimuthal vorticity increase from DNS data and through Crocco's theorem</b>	<b>179</b>
<b>C</b>	<b>Application of the oblique shock theory</b>	<b>182</b>
<b>D</b>	<b>Computation of average azimuthal vorticity increase</b>	<b>184</b>
	<b>Bibliography</b>	<b>186</b>

# List of Figures

1.1	Schematic showing the starting flow structures from under-expanded jets and over-expanded jets, respectively, emanating from a short nozzle.	2
1.2	Mach reflection and flow structures formed during the initial phases of an under-expanded jet. . . . .	3
2.1	Schematic of the physical domain for simulations and representative mesh of $210 \times 534$ grid-points in $z$ and $\tilde{r}$ directions. . . . .	25
2.2	Computational molecule around $i^{th}$ node . . . . .	32
2.3	Computational molecule on a grid line in $\tilde{r}$ direction showing grid points in the vicinity of pole ( $\tilde{r} = 0$ ) . . . . .	41
2.4	Density contours showing the starting phases of different compressible jets at $Re_j = 10^4$ obtained by employing the PVU-M+ scheme. . . . .	44
2.5	Density contours showing the flow-field of subsonic and supersonic jets at $Re_j = 10^4$ obtained from PVU-M+ scheme. . . . .	45
2.6	Density contours showing the starting phases of subsonic jet at $Re_j = 10^4$ and $M_j = 0.7$ obtained by employing the new features in the estimation of convective fluxes. . . . .	46
2.7	Density contours showing the starting phases of supersonic jet at $Re_j = 10^4$ and $M_j = 1.5$ obtained by employing the new features in the estimation of convective fluxes. . . . .	46
2.8	Density contours showing the flow-field of subsonic jets at $Re_j = 10^4$ and $M_j = 0.7$ obtained after employing inter-cell estimation of viscous fluxes. . . . .	48
2.9	Density contours showing the flow-field of supersonic jets at $Re_j = 10^4$ and $M_j = 1.5$ obtained after employing inter-cell estimation of viscous fluxes. . . . .	48
2.10	Numerical schlieren contours showing the starting flow structures formed in the subsonic jet at $Re_j = 10^4$ and $M_j = 0.7$ at different time instants.	49

2.11	Numerical schlieren contours showing the starting flow structures formed in the supersonic jet at $Re_j = 10^4$ and $M_j = 1.5$ at different time instants.	49
2.12	Numerical schlieren contours showing the starting flow structures formed in the under-expanded jets at $Re_j = 10^4$ and $M_j = 1.5$ (here, $PR$ means pressure ratio <i>i.e.</i> $\frac{p_j}{p_a}$ ).	50
2.13	Validation of time-histories of axial & radial coordinates of PVR for $\frac{P_j}{P_a} = 1$	51
2.14	Validation of time-histories of axial & radial coordinates of Mach-disk for $\frac{P_j}{P_a} = 1$	52
2.15	Validation of primary vortex core trajectories for $M_j = 1.4$ and $1.8$ , respectively.	53
2.16	Qualitative comparison of the formation of multiple vortex induced shocks (MVIS) between experimental schlieren visualizations of Ishii et al.[2] and numerical schlieren contours of present simulations.	54
2.17	Qualitative comparison of the Mach reflection, subsequent CRVR formation, formation of secondary Mach reflection and secondary Mach disk between the experimental schlieren visualizations of Haghdoost et al.[38] and numerical schlieren contours of present simulations.	56
2.18	Qualitative comparison of the Mach reflection, subsequent CRVR formation and formation of secondary slip-stream between numerical schlieren contours of Dora et al.[29] and the present study.	57
3.1	Numerical schlieren snapshots at different times for perfectly expanded jets with $Re_j = 10^4$ , $M_j = 1.5$ and $2.0$ , respectively.	62
3.2	Comparison of instantaneous schlieren snapshots for compressible starting jets at $Re_j = 10^4$ and $M_j = 1.5$ .	63
3.3	Numerical schlieren contours for transonic jets at $M_j = 0.9$ .	63
3.4	Comparison of the core bow shock data for two Reynolds numbers for the transonic jet at $M_j = 0.9$ .	64
3.5	Comparison of the core bow shock data for two Reynolds numbers for the transonic jet at $M_j = 1.5$ .	65
3.6	Instantaneous centreline pressure profiles depicting the effect of $M_j$ and $\frac{p_j}{p_a}$ at $t = 1$ at $Re_j = 10^4$ .	66
3.7	Variation of the centreline Mach number ( $M^c$ ) at the initial time instants for perfectly expanded jets at $Re_j = 10^4$ .	67
3.8	Contours of density, temperature, kinetic energy and Mach number showing the embedded shock in the PVR of a perfectly expanded jet at $Re_j = 10^4$ and $M_j = 1.5$ , at $t = 2$ .	69

3.9	Contours of density, temperature, kinetic energy and Mach number showing the embedded shock in the PVR of a perfectly expanded jet at $Re_j = 10^4$ and $M_j = 1.5$ , at $t = 6$ . . . . .	71
3.10	Numerical schlieren showing interaction of K-H vortex and embedded shock. . . . .	73
3.11	Numerical schlieren contours showing the K-H vortices inside the shear layer of compressible starting jets. . . . .	74
3.12	Numerical schlieren contours at different times showing details of K-H vortex and embedded shock interaction along with the appearance of multiple vortex induced shocks in a perfectly expanded jet at $Re_j = 10^4$ and $M_j = 1.5$ , respectively. . . . .	78
3.13	Contours of azimuthal vorticity ( $\Omega_{\bar{\theta}}$ ) at different times inside the PVR of a perfectly expanded jet at $Re_j = 10^4$ and $M_j = 1.5$ , respectively. . . . .	79
3.14	Temporal variation in the strength of embedded shock (ES) at the jet-centreline due to shock-vortex interaction (SVI) in the PVR of perfectly expanded jet at $Re_j = 10^4$ and $M_j = 1.5$ , respectively. . . . .	79
3.15	Numerical schlieren contours at different times in a perfectly expanded jet at $Re_j = 10^4$ and $M_j = 1.5$ , showing the formation time of K-H vortices in the shear layer. . . . .	81
3.16	Numerical schlieren images showing the effect of $Re_j$ on the interaction of K-H vortices with the embedded shock in the PVR of over-expanded/perfectly-expanded supersonic jets at $M_j = 1.5$ and $M_j = 2.0$ , respectively. . . . .	84
3.17	Numerical schlieren contours showing different stages of shock-shear layer vortex interaction in an under-expanded jet with $Re_j = 5 \times 10^4$ , $M_j = 1.5$ and $\frac{p_j}{p_a} = 3$ . . . . .	86
3.18	Numerical schlieren contours showing different stages of shock-shear layer vortex interaction in an under-expanded jet with $Re_j = 5 \times 10^4$ , $M_j = 1.5$ and $\frac{p_j}{p_a} = 1.5$ . . . . .	87
4.1	Figure showing slip-stream tangential velocity profile and its extraction method. . . . .	94
4.2	CRVR formation and evolution in an under-expanded jet having $M_j = 1.5$ , $\frac{p_j}{p_a} = 1.5$ at (a) $Re_j = 10^4$ and (b) $Re_j = 5 \times 10^4$ , respectively. . . . .	96
4.3	CRVR formation and evolution in an under-expanded jet having $M_j = 1.5$ , $\frac{p_j}{p_a} = 2$ at (a) $Re_j = 10^4$ (where $V_1, V_2, V_3$ and $V_4$ , respectively show the multiple CRVRs formed) and (b) $Re_j = 5 \times 10^4$ , respectively. . . . .	97

4.4	CRVR formation and evolution in an under-expanded jet having $M_j = 1.5$ , $\frac{p_j}{p_a} = 3$ at (a) $Re_j = 10^4$ (where $V_1$ , $V_2$ and $V_3$ , respectively show the multiple CRVRs formed) and (b) $Re_j = 5 \times 10^4$ , respectively. . . .	98
4.5	CRVR formation and evolution in an under-expanded jet having $M_j = 2$ , $\frac{p_j}{p_a} = 1.5$ at (a) $Re_j = 10^4$ and (b) $Re_j = 5 \times 10^4$ , respectively. . . . .	99
4.6	CRVR formation and evolution in an under-expanded jet having $M_j = 2$ , $\frac{p_j}{p_a} = 2$ at different jet Reynolds number ( $Re_j$ ). . . . .	101
4.7	CRVR formation and evolution in an under-expanded jet having $M_j = 2$ , $\frac{p_j}{p_a} = 3$ at different $Re_j$ . . . . .	102
4.8	Numerical schlieren showing straightening of the reflected shock in the Mach reflection due to $M_j$ increase in case of highly under-expanded jets at $Re_j = 10^4$ . . . . .	103
4.9	Block diagram showing the phenomenological model for single/multiple CRVR formation and formation of <i>CRVR</i> train along-with the effect of different non-dimensional parameters on them. . . . .	105
4.10	Schlieren images showing CRVR evolution in the moderately under-expanded jets at $M_j = 1.5$ and $\frac{p_j}{p_a} = 1.5$ at different $Re_j$ . . . . .	107
4.11	Schlieren images showing CRVR evolution in the highly under-expanded jets at $M_j = 1.5$ and $\frac{p_j}{p_a} = 2.0$ at different $Re_j$ . . . . .	108
4.12	Schlieren images showing the formation of discontinuities inside the <i>CRVRs</i> of under-expanded jets which involve multiple <i>CRVR</i> formation at different $Re_j$ . . . . .	110
5.1	Schematic showing the simply connected curve for circulation computation. . . . .	113
5.2	Time variation in the magnitude of rescaled circulation ( $\Gamma^r$ ) of primary vortex ring ( <i>PVR</i> ). . . . .	114
5.3	Numerical schlieren showing interaction between CRVR and vortex induced shock (VIS) in the under-expanded jets. . . . .	115
5.4	Time variation in the magnitude of rescaled circulation ( $ \Gamma^r $ ) of counter rotating vortex ring ( <i>CRVR</i> ). . . . .	116
5.5	The details of secondary Mach reflection in the moderately under-expanded jets at $\frac{p_j}{p_a} = 1.5$ . . . . .	118
5.6	Contours of azimuthal vorticity ( $\Omega_{\bar{\theta}}$ ) showing the evolution of the PVR in the under-expanded jet at $Re_j = 10^4$ , $M_j = 1.5$ and $\frac{p_j}{p_a} = 1.5$ . . . . .	119
5.7	Shock-shear layer-vortex interaction (SSVI) in the highly under-expanded jet at $Re_j = 10^4$ , $M_j = 1.5$ and $\frac{p_j}{p_a} = 2.0$ . . . . .	122

5.8	Streamlines shown over the density contours showing <i>CRVR</i> evolution in an under-expanded jet having $Re_j = 10^4$ , $M_j = 1.5$ and $\frac{p_j}{p_a} = 2$ . . . .	124
5.9	Density contours along-with plots of extracted-data of rescaled pressure, temperature and velocity for an induced shock (IS) inside <i>CRVR</i> of an under-expanded jet. . . . .	125
5.10	Density contours along-with plots of extracted-data of rescaled pressure, temperature and velocity for a vortex sheet (VS) inside <i>CRVR</i> of an under-expanded jet. . . . .	127
5.11	Streamlines shown over the density contours, showing the evolution of <i>CRVRs</i> in the under-expanded jet at $Re_j = 5 \times 10^4$ , $M_j = 1.5$ and $\frac{p_j}{p_a} = 2$ .	129
5.12	Streamlines shown over the density contours showing <i>CRVR</i> evolution in an under-expanded jet having $Re_j = 10^4$ , $M_j = 1.5$ and $\frac{p_j}{p_a} = 3$ . . . .	130
5.13	Contours of azimuthal vorticity ( $\Omega_{\hat{\theta}}$ ) showing the evolution of the <i>CRVR</i> in the under-expanded jet at $Re_j = 10^4$ , $M_j = 1.5$ and $\frac{p_j}{p_a} = 2.0$ . . . . .	131
5.14	Superposition of streamlines over contours of azimuthal vorticity ( $\Omega_{\hat{\theta}}$ ) at different times in the <i>CRVR</i> of an under-expanded jet having $Re_j = 10^4$ , $M_j = 1.5$ and $\frac{p_j}{p_a} = 2$ . . . . .	134
5.15	Interaction between <i>CRVR</i> and vortex induced shock (VIS) in a moderately under-expanded jet having $Re_j = 10^4$ , $M_j = 1.5$ and $\frac{p_j}{p_a} = 1.5$ . . .	135
5.16	Interaction between <i>CRVR</i> and vortex induced shock of an under-expanded jet having $Re_j = 10^4$ , $M_j = 1.5$ and $\frac{p_j}{p_a} = 3.0$ . . . . .	137
5.17	Interaction between <i>CRVR</i> and vortex induced shock of an under-expanded jet having $Re_j = 10^4$ , $M_j = 2.0$ and $\frac{p_j}{p_a} = 3.0$ . . . . .	137
5.18	Figure showing simply connected curve for computation of net-circulation and time variation in the rescaled net-circulation for different under-expanded jets. . . . .	139
6.1	Schematic showing the starting phases of an under-expanded jet emanating from a short nozzle into a co-flowing ambient fluid. . . . .	142
6.2	Effect of co-flow on the PVR, Mach reflection and <i>CRVR</i> formation in the moderately under-expanded jet at $\frac{p_j}{p_a} = 1.5$ for different velocity ratios. . . . .	144
6.3	Effect of co-flow on kinetic energy, temperature and local Mach number inside the shear layer and PVR of the moderately under-expanded jet at $\frac{p_j}{p_a} = 1.5$ . . . . .	146
6.4	Effect of co-flow on the PVR, Mach reflection and <i>CRVR</i> formation in the highly under-expanded jet at $\frac{p_j}{p_a} = 2.0$ . . . . .	147

6.5	Effect of co-flow on kinetic energy, temperature and local Mach number inside the shear layer and PVR of the highly under-expanded jet at $\frac{p_j}{p_a} = 2.148$	
6.6	Schematic showing P-M expansion fan (PMF), expansion fan angle ( $\theta$ ) and oblique shock (OS) inside the inviscid core of an under-expanded jet.	151
6.7	Effect of co-flow on rescaled pressure ( $p^r$ ) for the moderately under-expanded jet at $\frac{p_j}{p_a} = 1.5$ .	153
6.8	Effect of co-flow on local Mach number for the moderately under-expanded jet at $\frac{p_j}{p_a} = 1.5$ .	154
6.9	Effect of co-flow on the contours of rescaled pressure ( $p^r$ ) for the highly under-expanded jet at $\frac{p_j}{p_a} = 2.0$ .	157
6.10	Effect of co-flow on local Mach number for the highly under-expanded jet at $\frac{p_j}{p_a} = 2$ .	158
6.11	Figure showing simply connected curve for computation of PVR circulation and time variation in the rescaled PVR circulation for different under-expanded jets.	161
6.12	Streamlines superimposed over density contours at time $t = 3$ showing the effect of co-flow on the <i>PVR</i> in the under-expanded jet.	162
6.13	The occurrence of shock-shear layer-vortex interaction (SSVI) and entrainment of secondary slip-stream (SSS) into the <i>PVR</i> of the moderately under-expanded jet at $\frac{p_j}{p_a} = 1.5$ and $\frac{U_a}{U_j} = 0$ .	163
6.14	Different stages in the interaction of embedded shock (ES) and K-H vortices in the under-expanded jet at $\frac{p_j}{p_a} = 1.5$ and $\frac{U_a}{U_j} = 0.15$ , respectively.	165
6.15	Vorticity contours showing the distribution of azimuthal vorticity ( $\Omega_{\bar{\theta}}$ ) inside the <i>PVR</i> of the under-expanded jet at $\frac{p_j}{p_a} = 1.5$ and $\frac{U_a}{U_j} = 0.15$ , respectively.	166
6.16	Shock-vortex interaction between embedded shock and K-H vortex in the different under-expanded jets.	167
6.17	Shock-shear layer-vortex interaction in the highly under-expanded jet at $\frac{p_j}{p_a} = 2.0$ emanating into the co-flowing ambient at different velocity ratio (here, <i>VR</i> stands for velocity ratio).	168
A.1	Grid independence test for under-expanded jets	178
B.1	Superposition of streamlines over density contours showing methodology of data extraction for Crocco's theorem.	180
C.1	Superposition of streamlines over density contours at $t = 8.5$ for application of the oblique shock theory in an under-expanded jet at $Re_j = 5 \times 10^4$ , $M_j = 1.5$ and $\frac{p_j}{p_a} = 3.0$ .	183

D.1 Streamlines shown over the density contours (at time  $t = 9$ ) alongwith the upstream (1) and downstream (2) locations where average azimuthal vorticity jump ( $\Delta\Omega_{\bar{\theta}}$ ) is computed across (a) the induced shock (IS) and (b) the vortex sheet (VS) inside the *CRVR* of an under-expanded jet with  $Re_j = 10^4$ ,  $M_j = 1.5$  and  $\frac{p_j}{p_a} = 2$ . . . . . 185

# List of Tables

1.1	The parametric space investigated in the present study . . . . .	14
2.1	Scales employed for non-dimensionalization . . . . .	20
2.2	Details of the computational grids employed in simulations. . . . .	26
2.3	Application of algebraic characteristic boundary conditions (AECBC) in subsonic flows for different wave types. . . . .	30
2.4	Application of algebraic characteristic boundary conditions (AECBC) in supersonic flows for different wave types. . . . .	30
2.5	Magnitude of the various filter coefficients . . . . .	43
2.6	Parameteric space of Ishii et al.[2] ( <i>IFHU</i> ) used in benchmarking the code. . . . .	51
2.7	Parameteric space of Zhang et al.[4] ( <i>ZCLJ</i> ) used in benchmarking the code. . . . .	51
3.1	Effects of $M_j$ on transient core bow shock characteristics at different times in subsonic/supersonic jets at $Re_j = 10^4$ and $\frac{p_j}{p_a} = 1$ . . . . .	68
3.2	Effects of $\frac{p_j}{p_a}$ on transient core bow shock characteristics at $t_1 = 1, t_2 = 2$ for supersonic jets at $Re_j = 10^4$ and $M_j = 1.5$ . . . . .	68
3.3	Variation of the instantaneous strength ( $p_{ds}^r/p_{us}^r$ ) of ES and VIS with $M_j$ at different time instants for perfectly expanded supersonic jets at $Re_j = 10^4$ . . . . .	70
3.4	Variation of the instantaneous strength ( $p_{ds}^r/p_{us}^r$ ) of ES and VIS with $\frac{p_j}{p_a}$ at different time instants for supersonic jets at $Re_j = 10^4$ and $M_j = 1.5$ , respectively. . . . .	71
3.5	Variation with $M_j$ in the dimensionless rescaled <i>PVR</i> circulation ( $\Gamma^r$ ) for perfectly expanded jets with $Re_j = 10^4$ at different times. . . . .	75
3.6	Variation with $\frac{p_j}{p_a}$ in dimensionless rescaled <i>PVR</i> circulation ( $\Gamma^r$ ) for supersonic jets with $Re_j = 10^4$ and $M_j = 1.5$ at $t = 6$ . . . . .	76

3.7	Comparison of <i>DNS</i> data and <i>Crocco's theorem</i> prediction for average azimuthal vorticity increase ( $\Delta\bar{\Omega}_{\hat{\theta}}$ ) across different shocks in the evolving <i>PVR</i> of a perfectly expanded jet at $Re_j = 10^4$ and $M_j = 1.5$ , respectively. . . . .	82
3.8	Vorticity jumps across the incident and refracted portions of the oblique shock and across different shocks in the evolving <i>PVR</i> of an under-expanded jet at $Re_j = 5 \times 10^4$ , $M_j = 1.5$ and $\frac{p_j}{p_a} = 3$ . . . . .	88
3.9	Comparison of angle ( $\theta$ ) with which the incoming flow is deflected by the reflected oblique shock and its refracted portion as obtained using the oblique shock theory ( <i>OST</i> ) and from the simulations. . . . .	89
4.1	Variation in Mach-disk strength ( $[p_{ds}^r/p_{us}^r]_{MD}$ ), oblique shock strength ( $[p_{ds}^r/p_{us}^r]_{OS}$ ), slip-stream strength ( $\partial V_t/\partial n$ ) and time-span of Mach reflection ( $\Delta t_{MR}$ ) with $M_j$ , $\frac{p_j}{p_a}$ during the Mach reflection in the starting under-expanded jets at different $Re_j$ . . . . .	93
5.1	Average azimuthal vorticity increase ( $\Delta\bar{\Omega}_{\hat{\theta}}$ ) or vorticity production across the <i>PVR</i> shock-system alongwith the comparison of azimuthal vorticity fluxes ( $V_{\hat{r}}\Omega_{\hat{\theta}}$ ) through the shear layer ( <i>SL</i> ) and secondary slip-stream ( <i>SSS</i> ) into the unpinched <i>PVR</i> ( <i>i.e.</i> control region $S'$ ) of a moderately under-expanded jet at $Re_j = 10^4$ , $M_j = 1.5$ and $\frac{p_j}{p_a} = 1.5$ . . . . .	120
5.2	Vorticity production across the <i>PVR</i> shock-system alongwith the azimuthal vorticity flux ( $V_{\hat{r}}\Omega_{\hat{\theta}}$ ) through the shear layer ( <i>SL</i> ) into the <i>PVR</i> of the under-expanded jet at $Re_j = 10^4$ , $M_j = 1.5$ and $\frac{p_j}{p_a} = 2$ . . . . .	123
5.3	Temporal variation with time in the strength ( $p_2^r/p_1^r$ ) of induced shock ( <i>IS</i> ). . . . .	128
5.4	Variation in induced shock strength ( $p_2^r/p_1^r$ ) with $M_j$ and $\frac{p_j}{p_a}$ . . . . .	128
5.5	Variation in the <i>DNS</i> data for average azimuthal vorticity increase ( $\Delta\bar{\Omega}_{\hat{\theta}}$ ) across the induced shocks and vortex sheet alongwith the azimuthal vorticity flux ( $V_{\hat{r}}\Omega_{\hat{\theta}}$ ) through the slip-stream ( <i>SS</i> ) into the evolving <i>CRVR</i> . . . . .	132
5.6	Temporal variation in the increase/jump in different fluid-properties across <i>VIS</i> and change in the magnitude of <i>CRVR</i> circulation during shock-vortex interaction in the under-expanded jet with $Re_j = 10^4$ , $M_j = 1.5$ and $\frac{p_j}{p_a} = 1.5$ . . . . .	136

5.7	Temporal variation in the increase/jump in different fluid-properties across VIS and change in the magnitude of CRVR circulation during shock-vortex interaction in the under-expanded jet with $Re_j = 10^4$ , $M_j = 1.5$ and $\frac{p_j}{p_a} = 3.0$ . . . . .	136
6.1	Variation with co-flow ( $\frac{U_a}{U_j}$ ) in the average tangential velocity jump ( $\frac{\bar{V}_{t_{core}}}{\bar{V}_{t_{amb}}}$ ) across the shear layer of under-expanded jets. . . . .	143
6.2	Variation in the strength ( $p_{ds}^r/p_{us}^r$ ) of embedded shock (ES) and vortex induced shock (VIS) with velocity ratio ( $\frac{U_a}{U_j}$ ) in the moderately under-expanded jet at $\frac{p_j}{p_a} = 1.5$ . . . . .	143
6.3	Variation in the strength ( $p_{ds}^r/p_{us}^r$ ) of embedded shock (ES) and vortex induced shock (VIS) with velocity ratio ( $\frac{U_a}{U_j}$ ) in the highly under-expanded jet at $\frac{p_j}{p_a} = 2$ . . . . .	149
6.4	Variation in oblique shock strength ( $[p_{ds}^r/p_{us}^r]_{OS}$ ), Mach-disk strength ( $[p_{ds}^r/p_{us}^r]_{MD}$ ), embedded shock strength ( $[p_{ds}^r/p_{us}^r]_{ES}$ ) (computed inside the inviscid core), slip-stream strength ( $\partial V_t/\partial n$ ) and time-span of Mach reflection ( $\Delta t_{MR}$ ) with the velocity-ratio ( $\frac{U_a}{U_j}$ ) during the Mach reflection in the moderately under-expanded jet at $\frac{p_j}{p_a} = 1.5$ . . . . .	150
6.5	During Mach reflection, variation with co-flow ( $\frac{U_a}{U_j}$ ) in the expansion fan angle ( $\theta$ ) and flow conditions prevailing downstream of expansion fan (at location 2) for the jet at $\frac{p_j}{p_a} = 1.5$ . . . . .	151
6.6	Variation with co-flow ( $\frac{U_a}{U_j}$ ) in the rescaled average advection speed ( $U_{PS}^r$ ) and strength of the precursor shock ( $PS$ ) at $t = 1$ in the moderately under-expanded jet at $\frac{p_j}{p_a} = 1.5$ . . . . .	154
6.7	Variation in oblique shock strength ( $[p_{ds}^r/p_{us}^r]_{OS}$ ), Mach-disk strength ( $[p_{ds}^r/p_{us}^r]_{MD}$ ), embedded shock strength ( $[p_{ds}^r/p_{us}^r]_{ES}$ ) (computed inside the inviscid core), slip-stream strength ( $\partial V_t/\partial n$ ) and time-span of Mach reflection ( $\Delta t_{MR}$ ) with the velocity-ratio ( $\frac{U_a}{U_j}$ ) during the Mach reflection in the highly under-expanded jet at $\frac{p_j}{p_a} = 2$ . . . . .	155
6.8	During Mach reflection, variation with co-flow ( $\frac{U_a}{U_j}$ ) in the expansion fan angle ( $\theta$ ) and flow conditions prevailing downstream of expansion fan (at location 2) for the jet at $\frac{p_j}{p_a} = 2.0$ . . . . .	156
6.9	Variation with co-flow ( $\frac{U_a}{U_j}$ ) in the rescaled average advection speed ( $U_{PS}^r$ ) and strength of the precursor shock ( $PS$ ) at $t = 1$ in the highly under-expanded jet at $\frac{p_j}{p_a} = 2.0$ . . . . .	158

6.10	Average azimuthal vorticity increase ( $\Delta\bar{\Omega}_{\tilde{\theta}}$ ) across the PVR shock-system alongwith the comparison of azimuthal vorticity flux ( $V_{\tilde{r}}\Omega_{\tilde{\theta}}$ ) through the shear layer ( $SL$ ) and secondary slip-stream ( $SSS$ ) into the unpinched PVR ( <i>i.e.</i> control region $S'$ ) of the under-expanded jet at $\frac{p_j}{p_a} = 1.5$ and $\frac{U_a}{U_j} = 0$ . . . . .	164
6.11	Vorticity production across the system of different shocks during shock-vortex interaction (SVI) in the under-expanded jet at $\frac{p_j}{p_a} = 1.5$ and $\frac{U_a}{U_j} = 0.15$ , respectively. . . . .	166
6.12	Vorticity production across the system of different shocks during the shock-shear layer-vortex interaction in the under-expanded jet at $\frac{p_j}{p_a} = 2$ and $\frac{U_a}{U_j} = 0.15$ , respectively. . . . .	168

# Nomenclature

$d$	:	filter coefficients
$r$	:	radial coordinate
$\theta$	:	azimuthal coordinate
$z$	:	axial coordinate
$\tilde{r}$	:	transformed radial coordinate
$\tilde{\theta}$	:	transformed azimuthal coordinate
$\delta$	:	boundary layer thickness
$F^*$	:	formation number
$Re_j$	:	jet Reynolds number
$Pr_j$	:	jet-fluid Prandtl number
$M_j$	:	jet Mach number
$M_s$	:	shock Mach number
$\frac{p_j}{p_a}$	:	pressure ratio
$\frac{p_r}{p_a}$	:	reservoir pressure ratio
$\frac{\rho_j}{\rho_a}$	:	density ratio
$\frac{T_j}{T_a}$	:	temperature ratio
$\frac{U_a}{U_j}$	:	velocity ratio
$D_j$	:	jet diameter
$U_j$	:	jet exit velocity
$U_a$	:	ambient fluid velocity
$T_a$	:	ambient temperature
$\rho_a$	:	ambient density
$U$	:	solution vector
$F$	:	radial flux vector
$H$	:	axial flux vector
$J$	:	source vector
$\tilde{U}$	:	solution vector in transformed coordinates
$\tilde{F}$	:	radial flux vector in transformed coordinates
$\tilde{H}$	:	axial flux vector in transformed coordinates
$\tilde{J}$	:	source vector in transformed coordinates

$\rho$	:	density
$V_r$	:	radial velocity
$V_{\bar{r}}$	:	transformed radial velocity
$V_z$	:	axial velocity
$E$	:	total energy
$p$	:	pressure
$e$	:	specific internal energy
$T$	:	temperature
$s$	:	entropy
$h_T$	:	total enthalpy
$S_\mu, S_k$	:	Sutherland constants
$T_0, T_{0k}$	:	reference temperature
$B_r, B_z$	:	components of body force field
$Re$	:	flow Reynolds number
$M$	:	flow Mach number
$Pr$	:	flow Prandtl number
$Fr$	:	Froude number
$C_p, C_v$	:	specific heat constants
$N_r$	:	number of grid points in radial direction
$N_z$	:	number of grid points in axial direction
$i, j$	:	grid indices
$c$	:	local speed of sound
$\mathbf{Q}$	:	convection property vector
$W$	:	characteristic speed
$W_f$	:	weight function
$u_{sn}$	:	normal flow velocity magnitude
$R$	:	universal gas constant
$R^+, R^-$	:	Riemann invariants
$p_{ds}^r$	:	rescaled pressure downstream
$p_{us}^r$	:	rescaled pressure upstream
$p^r$	:	rescaled pressure
$p_c^r$	:	rescaled centreline pressure
$M^c$	:	centreline Mach number
$U^r$	:	rescaled average advection speed
$c_j$	:	sonic speed at the exit
$\frac{p_{ds}^r}{p_{us}^r}$	:	shock strength
$\hat{n}$	:	local normal vector

$\alpha$	:	fluid property
$\beta$	:	grid point condensation parameter
$\phi$	:	inter-cell convective property vector
$\phi_l$	:	relative advection coefficient
$\eta$	:	weights used in discrete approximations
$\lambda$	:	wave speed
$k$	:	coefficient of thermal conductivity
$\mu$	:	coefficient of viscosity
$\tau_{ij}$	:	viscous stress tensor
$\tau_{rr}$	:	viscous stress tensor component
$\tau_{rz}$	:	viscous stress tensor component
$\tau_{zz}$	:	viscous stress tensor component
$\tau_{\theta\theta}$	:	viscous stress tensor component
$\tau_{\tilde{r}\tilde{r}}$	:	viscous stress tensor components in tranformed coordinates
$\tau_{\tilde{r}z}$	:	viscous stress tensor components in tranformed coordinates
$\tau_{zz}$	:	viscous stress tensor components in tranformed coordinates
$\tau_{\tilde{\theta}\tilde{\theta}}$	:	viscous stress tensor components in tranformed coordinates
$\gamma$	:	specific heat ratio
$\Gamma$	:	circulation
$\Gamma^r$	:	rescaled circulation
$\Gamma_{net}^r$	:	net-rescaled circulation
$\vec{\Omega}$	:	vorticity
$\Omega_{sep}$	:	seperation vorticity
$\Omega_{corePVR}$	:	PVR core vorticity
$\Omega_{\tilde{\theta}}$	:	azimuthal vorticity
$\Delta\overline{\Omega}_{\tilde{\theta}}$	:	average azimuthal vorticity increase across a shock
$\frac{\partial V_t}{\partial n}$	:	slip-stream strength

## Abbreviations

AECBC	:	algebraic Euler characteristic boundary conditions
CBS	:	core bow shock
CBUE	:	continuously blowing under-expanded jets
CRVR	:	counter rotating vortex ring
CSVR	:	co-rotating secondary vortex ring
DNS	:	direct numerical simulation
EF	:	expansion fan
ES	:	embedded shock
I	:	shock-tube exit impulse
IOS	:	incident oblique shock
IS	:	induced shock
ISL	:	induced shock location
ISK	:	incident shocks
KHV	:	Kelvin-Helmholtz vortices
HPR	:	high pressure region
LES	:	large eddy simulation
LPR	:	low pressure region
MD	:	Mach disk
MPI	:	Message Passing Interface
MR	:	Mach Reflection
MS	:	Mach stem
OS	:	oblique shock
OST	:	oblique shock theory
PMF	:	Prandtl Meyer expansion fan
PC	:	PVR core axial location
PG	:	pressure gradient
PIV	:	particle image velocimetry

PO	:	pinch-off point
PS	:	precursor shock
PVR	:	primary vortex ring
PVU-M+	:	Particle Velocity Upwind Modified+
PVU-M+J	:	Particle Velocity Upwind Modified+Jets
ROS	:	reflected oblique shock
RSK	:	reflected shock
SCS	:	shock-cell structure
SD	:	saddle stagnation point
SN	:	short nozzle
SMD	:	secondary Mach disk
SP	:	spiral stagnation point
SPI	:	shear layer-PVR interface
SL	:	shear layer
SS	:	slip-stream
SSS	:	secondary slip-stream
STP	:	secondary triple point
SVI	:	shock-vortex interaction
SSVI	:	shock-shear layer-vortex interaction
STGI	:	shock-tube generated impulsive jets
VIS	:	vortex induced shock
VS	:	vortex sheet
VRES	:	vortex ring embedded shock